Conformational stability, barriers to internal rotation of 2-aminothiophenol (d0 and d3): A combined vibrational and theoretical approach

ARTICLE *in* JOURNAL OF MOLECULAR STRUCTURE THEOCHEM · SEPTEMBER 2008

Impact Factor: 1.37 · DOI: 10.1016/j.theochem.2008.06.021

4 AUTHORS:

Tarek Mohamed
Al-Azhar University
48 PUBLICATIONS **373** CITATIONS
SEE PROFILE

Usama Soliman
Al-Azhar University
11 PUBLICATIONS **32** CITATIONS
SEE PROFILE

Ahmed Hanafy
16 PUBLICATIONS **99** CITATIONS
SEE PROFILE

Ali M. A. Hassan
Al-Azhar University
43 PUBLICATIONS **147** CITATIONS
SEE PROFILE

Journal of Molecular Structure: THEOCHEM 865 (2008) 14–24

Contents lists available at ScienceDirect

Journal of Molecular Structure: THEOCHEM

journal homepage: www.elsevier.com/locate/theochem

Conformational stability, barriers to internal rotation of 2-aminothiophenol (d_0 and d_3): A combined vibrational and theoretical approach

Tarek A. Mohamed *, Usama A. Soliman [1], Ahmed I. Hanafy, Ali M. Hassan

Department of Chemistry, Faculty of Science (Men's Campus), El Mokhayium El Daiem, Al-Azhar University, Nasr City, Cairo 11884, Egypt

ARTICLE INFO

Article history:
Received 10 February 2008
Received in revised form 18 May 2008
Accepted 12 June 2008
Available online 2 July 2008

Keywords:
2-Aminothiophenol
Vibrational spectra
Normal coordinate analysis
Barriers to internal rotation and *ab initio* calculations

ABSTRACT

The Raman (3700–100 cm^{-1}) and infrared (4000–400 cm^{-1}) spectra of liquid 2-aminothiophenol (2ATP) have been recorded and complemented with quantum mechanical calculations. Ten rotational isomers (C_s and/or C_1 symmetry) have been considered due to the rotation of NH_2 moiety around C–N bond, while the in-plane SH group is directed towards and/or away from NH_2, respectively. Initial computational results are in favor of two conformers where the SH group is directed towards the NH_2 moiety with C_1 symmetry (**7**; *gauche-1*, **8**; *trans*). An additional *gauche-2* isomer (**11**) was revealed; with NH_2 moiety perpendicular to the benzene ring and the out-of-plane SH group is directed towards NH_2 while the lone pairs of electrons on nitrogen and sulfur atoms reside in opposite directions. From MP2/6-31G(d) calculations, the *gauche-2* (**11**) is predicted to be more stable than *trans* (**8**) and *gauche-1* (**7**) by 758 (2.17 kcal/mol) and 833 cm^{-1} (2.38 kcal/mol), respectively. Aided by theoretical and experimental outcomes, *gauche-2* (**11**) conformer appears to dominate the liquid phase with minor spectroscopic features relating to *gauche-1* (**7**) and/or *trans* (**8**) conformers. Aided by normal coordinate analysis, force constants and frequency calculations, a complete vibrational assignment has proposed for 2ATP ($HSC_6H_4NH_2$) and its deuterated analogue ($DSC_6H_4ND_2$). The structural parameters were optimized without any constrains with the addition of polarization and diffusion functions at 6-311+G(d) and 6-31++G(d,p) basis sets using RHF, MP2 and B3LYP, all in favor of *gauche-2* (**11**) conformer. Additionally, the SH and NH_2 barriers to internal rotations have been considered for 2-aminothiophenol and compared with 2-aminophenol (2AP).

1. Introduction

Organic materials like 2-aminothiophenol (2ATP) and its derivatives are used in corrosion inhibition processes due to their predicted adsorbing characteristics of the lone pair electrons on the thiol and amine moieties as well as the π electrons of the benzene ring [1,2]. The absorbance of 2ATP has been used to probe the electromagnetic enhancement mechanisms of surface enhanced Raman spectra. Moreover, the reactivity of transition metal complexes containing nitrogen–sulfur donor atoms is not only important for academic reasons but also for the last two decade became potential antibacterial, antifungal and anticancer agents [3–5]. Vibrational spectroscopy supported by molecular modeling calculations is considered the most important method for structural characterization. It can be used to characterize environmental influences, periodic trends in terms of subsistent groups [6–8], as well as inter- and intramolecular hydrogen bonding [9,10]. The thermodynamic and electrical properties [11–13] as well as vibrational spectra (IR, R, SERS) of aniline and its derivatives have been already investigated [14–18]. A prerequisite to characterize the vibrational features of 2ATP is a careful analysis of its oxygen homologue, i.e., 2-aminophenol (2AP) which assists in overcoming the controversial interpretation of certain vibrational modes below 1000 cm^{-1} [15,17]. The vibrational spectra and conformational stability of 2AP and 2ATP were in favor of *cis* (OH directed towards NH_2) and *trans* (OH directed away from NH_2) isomers with C_s symmetry [11,16,17] but Usama et al. had identified extra possible conformations [19]. Similar to 2AP, the structural and energetic implications of 2ATP is not yet considered. To the best of our knowledge, normal coordinate analysis (NCA), SH and NH_2 barriers to internal rotation have yet been explored.

We aim to take advantage of quantum mechanical (QM) calculations to support and complement infrared (IR) and Raman (R) spectra of 2ATP. Accordingly, we have applied LCAO-MO-SCF Gaussian 98 *ab initio* calculations [20] using the levels of RHF, MP2 and B3LYP [21–27] at standard basis sets up to 6-31++G(d,p). Polarization and diffusion functions are tested to investigate basis set convergence of geometries, vibrational fre-

* Corresponding author. Tel.: +202 37200773; fax: +202 22629356.
E-mail address: tarek_ama@hotmail.com (T.A. Mohamed).

[1] Taken in part from the Master Thesis of Usama A. Soliman which was submitted to Chemistry Department, Faculty of Science, Al Azhar University, Nasr City, Cairo 11884, Egypt.

0166-1280/$ - see front matter © 2008 Elsevier B.V. All rights reserved.
doi:10.1016/j.theochem.2008.06.021

quencies, harmonic force constants (FCs), infrared intensities and Raman activities. The results are reported herein and compared to other similar molecules whenever appropriate.

2. Experimental

The sample of 2ATP ($HSC_6H_4NH_2$), 99% grade was obtained from Aldrich Chemical Company, Egypt branch and has been used without further purification. Raman spectroscopic measurements are measured using Fourier Transform Raman (FT-R) accessories at the National Research Center, Dokki, Cairo, Egypt. The Raman spectrum of liquid 2ATP (Fig. 1) was recorded on a Nexus-670- Nicolet FT-R spectrometer in the range of 3700–100 cm^{-1}. The Raman spectrophotometer is equipped with 1064 nm Nd:Y:Ag laser of ~0.48–0.5 W for excitation at 64 scans. A liquid sample was dropped on the surface of KBr then the IR spectrum is recorded at once using FT Perkin Elmer (Spectrum RX), forty scans were collected utilizing 4 cm^{-1} resolution in the region of 4000–400 cm^{-1} (Fig. 2). The recorded Raman (R) and infrared (IR) spectra of 2ATP are almost identical to those obtained by Griffith [17] but the frequencies differ by ±8 cm^{-1}. The observed R and IR spectral data of $HSC_6H_4NH_2$ and $DSC_6H_4ND_2$ are summarized in Table 1.

3. *Ab initio* calculations

For 2ATP, we carried out Gaussian 98 quantum mechanical (QM) calculations [20,21] for all possible rotational isomers at the levels of Restricted Hartree–Fock (RHF), Moller–Plesset second perturbation (MP2) and Becke three Lee–Yang–Parr parameters (B3LYP) utilizing 6-31G(d) basis set [21–26]. The optimized structural parameters (SPs) are obtained by simultaneous relaxation of all the geometric parameters by using the gradient method of Pulay [27]. Structural optimization strategies are described below and were continued up to reaching the convergence criteria implemented in Gaussian 98 (maximum force of 0.000450 mdyne where RMS (root mean square) force 0.000300 mdyne and maximum displacement of 0.001800 Å where RMS displacement is 0.001200 Å [20]. Then, the attained SPs have been used to calculate the harmonic vibrational frequencies utilizing the same level and basis set. Moreover, larger basis sets up to 6-31G++(d,p) have been used to account for polarization and diffusion interactions [21]. The results are compared with earlier MP2 and B3LYP levels at 6-31G(d) basis set for 2AP whenever appropriate.

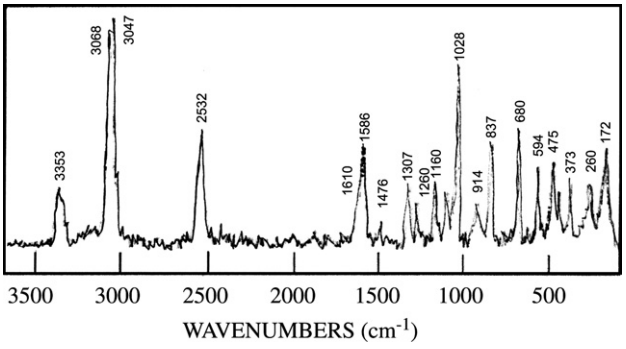

Fig. 1. Raman spectrum of liquid 2ATP in the region of (100–3700 cm^{-1}).

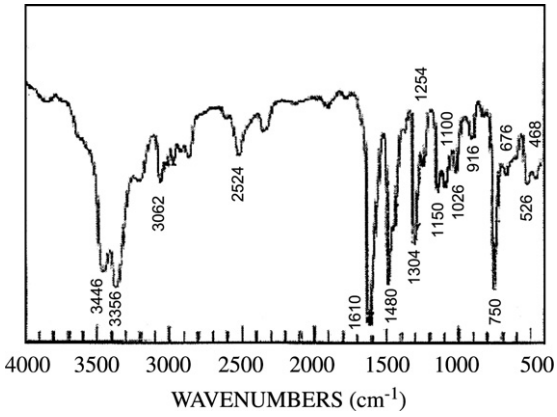

Fig. 2. Mid-infrared spectrum of liquid 2ATP in the region of (400–4000 cm^{-1}).

3.1. Rotational isomerism

As in 2-aminophenol [19], 2ATP is considered to have a dual internal rotors (SH and NH_2), therefore either SH or NH_2 moiety was fixed while rotating the other to produce isomers presented in Figs. 3 and 4. Conformer **1**; *cis* (Fig. 3) and conformer **6**; *trans* (Fig. 4) result when the SH group directed towards and away from NH_2 moiety, respectively. To maintain C_s symmetry of **1** and **6**, all atoms are kept in plane except the two N–H bonds. Four isomers **2**, **3**, **4** and **5** (Fig. 3) are produced by rotating the NH_2 group of *cis* (**1**) conformer around the C–N bond by C_6, C_3, C_2 and C_n ($0° < n < 60°$). Similarly, the NH_2 moiety of isomer **6** has been rotated to generate **7** (*gauche-1*), **8** (*trans*), **9** and **10** isomers (Fig. 4). The MP2/6-31G(d) structural parameters for **7**, **8** and **11** conformers of 2ATP utilizing 6-31G(d), 6-311+G(d) and 6-31++G(d,p) basis sets are given in Table 2, whereas the predicted SPs from B3LYP level are listed in Supplementary Table A, respectively. Owing to the predicted imaginary frequencies as well as their relatively high energies, the underlined isomers **1**, **2**, **3**, **4**, **5**, **6**, **9**, **10** are considered transition states. As a consequence, we are focused on *gauche-1* (**7**) and *trans* (**8**) isomers, with conformer **8** being more stable than **7** by 758 cm^{-1}. For *trans* (**8**), the NH_2 group is perpendicular (⊥) to the benzene ring while the two NH bonds and lone pair electrons are out-of-plane). On the other hand, transition states result in case of SH moiety is ⊥ to the benzene ring and NH_2 group exhibit SP^2 hybridization (Supplementary Fig. A). These isomers have been excluded owing to the prediction of negative frequencies as well as their relative high energies.

For, 2ATP, three conformers having C_1 symmetry are fully converged with real frequencies (**7**; *gauche-1*, **8**; *trans* and **11**; *gauche-2*). Their relative energy differences (ΔE) up to 6-31++G(d,p) basis set employing various levels are summarized in Table 3. It is worth mentioning that, calculated energies of 2ATP are found to be lower than those of 2AP [19] at the same level and basis set of calculations. The fully converged isomers in case of 2AP were deviated from those identified for 2ATP. No minimum conformation was achieved for 2AP with OH moiety being out-of-plane. For comparative purposes, B3LYP vibrational frequencies, IR intensities and Raman activities for *gauche*-2 (**11**) and *trans* (**8**) isomers are given in Supplementary Table B.

3.2. OH, SH and NH_2 barriers to internal rotations

To justify the conformational stability of 2ATP, we have also utilized a potential surface scan (PSS) using MP2/6-31G(d) optimized SPs for *trans* (**8**) conformer where dihedral angle HSC_1C_{11} (τ_1) is chosen to be zero with an energy of −684.2810837 Hartree (Fig. 4). Then the SH group was rotated by 10° increments around C–S bond while NH_2 group was held fixed at dihedral angles of 43.0° and 12.1° for $H_{15}N_4C_3C_1$ (τ_2) and $H_{14}N_4C_3C_5$ (τ_3), respectively (Fig. 5). When SH rotates by 10° increments, the energy increases gradually till reaching a maximum at τ_1 of 50° (E = −684.27856 Hartree) with SH barrier to internal rotation of

Table 1
Observed and calculated MP2/6-31G(d) wavenumbers and potential energy distributions for *gauche-2* (**11**) *ortho*-aminothiophenol

No.	Fundamental	*Gauche-2 ortho*-$HSC_4H_6NH_2$								PED[f]	*Gauche-2 ortho*-$DSC_4H_6ND_2$				PED[f]
		Ab initio[a]	Fixed scaled[b]	IR Int.[c]	R act.[d]	Obs.[e] Ref. [17]		This study			*Ab initio*[a]	Fixed scaled[b]	Obs.[e] Ref.[17]		
						IR_{liquid}	R_{liquid}	IR_S	R_S				IR_S	R_S	
ν_1	$\upsilon_{as}(NH_2/ND_2)$	3659	3472	18.4	49. 9	3449s	3432w	3446vs	(3353m)	98 S_1	2701	2563	–	2494sh	99 S_1
ν_2	$\upsilon_s(NH_2/ND_2)$	3541	3360	17.8	134.8	3357vs	3358w	3356vs	(3353m)	$98S_2$	2561	2430	2408vs	2446m	$99S_2$
ν_3	υ_s(CH)	3250	3168	13.7	202.1	3064m	3068vs	3062m	3086vs	$73S_3$ $15S_6$ $11S_4$	3250	3168	3060vs	3086vs	$73S_3$ $15S_6 11S_4$
ν_4	υ_s(CH)	3235	3153	12.2	63.6	–	3050vs	–	3047vs	$72S_4$ $26S_6$	3235	3253	–	3046vs	$72S_4$ $26S_6$
ν_5	υ_s(CH)	3227	3146	1.1	84.6	(3018m)	(3022sh)	(3010msh)	(3021sh)	$49S_5$ $27S_6$ $16S_3$	3227	3146	3016vs	3024vw	$49S_5$ $27S_6$ $16S_3$
ν_6	υ_s(CH)	3209	3128	8.3	63.7	(3018m)	(3022sh)	(3010msh)	(3021sh)	$31S_6$ $51S_5$ $10S_3$	3209	3127	–	–	$31S_6$ $51S_5$
ν_7	υ_s(SH/SD)	2755	2614	5.4	117.6	2524m	2532m	2524mbr	2532s	$100S_7$	1978	1877	1835m	1840w	$100S_7$
ν_8	$\delta_{scissors}(NH_2/ND_2)$	1706	1648	108.7	18.2	1610vs	1610msh	(1610vsbr)	1610m	$60S_8$ $17S_{26}$	1208	1158	1130s	1130w	$35S_8$ $18S_{26}$ $16S_{11}12S_{16}$
ν_9	Ring stretch	1670	1613	4.5	15.2	1585sh	1586s	(1610vsbr)	1586m	$34S_9$ $15S_{19}$ $14S_8$ $11S_{14}$	1677	1639	1591w	1590s	$42S_9$ $23S_{19}$ $12S_4$
ν_{10}	Ring stretch	1654	1606	2.3	7.8	1574sh	1572sh	(1610vsbr)	1574sh	$49S_{10}$ $14S_{17}$ $11S_{16}$	1648	1607	1561sh	1570sh	$50S_{10}$ $18S_{17}$ $12S_{16}$
ν_{11}	δ(CH) in-plane	1550	1515	55.9	1.9	1481vs	1480w	1480vs	1476w	$49S_{11}$ $17S_{19}$ $11S_9$ $10S_{15}$	1547	1514	1476vs	1478w	$38S_{11}$ $20S_{19}11S_9 10S_{15}$
ν_{12}	δ(CH) in-plane	1509	1473	18.4	1.2	1448vs	1448w	1448ssh	1440vw	$44S_{12}$ $25S_{17}$	1504	1470	1444vs	1446w	$45S_{12}$ $24S_{17}$ $10S_{10}$
ν_{13}	Ring stretch	1472	1432	6.7	6.8	1385w	1390vw	1400sh	–	$88S_{13}$	1462	1424	–	1392vw	$88S_{13}$
ν_{14}	δ(CH) in-plane	1357	1329	17.2	6.5	1307vs	1306m	1304s	1307m	$36S_{14}$ $20S_{15}$ $18S_{12}$	1311	1279	1252vs	1252w	$56S_{14}$ $10S_{19}$
ν_{15}	υ(C–N)	1315	1287	5.5	7.0	1251m	1258w	1254msh	1260m	$24S_{15}$ $24S_{14}$ $14S_{11}$ $10S_{20}$	1370	1343	1314vs	1308m	$16S_8$ $14S_{14}$ $12S_{12}$
ν_{16}	δ(CH) in-plane	1217	1186	2.1	4.9	1159s	1162w	(1150s)	1160m	$60S_{16}$ $22S_{11}$	1219	1186	1162s	1156w	$56S_{16}$ $12S_8$
ν_{17}	δ(CH) in-plane	1198	1164	3.1	5.4	1142m	1144vs	(1150s)	1153sh	$18S_{17}$ $24S_{14}$ $20S_{12}$ $19S_{18}$	1182	1154	1149s	1141w	$35S_{17}28S_{12}13S_{14}$
ν_{18}	$\delta_{twist}(NH_2/ND_2)$	1147	1115	8.3	5.5	1089m	1082s	1100s	1088m	$36S_{18}$ $17S_{17}$ $15S_{28}$	907	876	850sh	830w	$73S_{18}$
ν_{19}	Ring stretch	1096	1070	1.0	3.2	1049m	1052wsh	–	1056w	$25S_{19}$ $22S_{24}$ $17S_{11}$ $11S_9$	1081	1056	1032s	1036vs	$13S_{19}$ $47S_{20}$ $11S_{28}$
ν_{20}	δ(CCC)	1069	1043	6.8	18.2	1026s	1028vs	1026sbr	1028vs	$34S_{20}$ $31S_{24}$	1096	1076	1062m	1052w	$42S_{20}$ $12S_{19}$ $12S_{24}$ $10S_{11}$
ν_{21}	δ(SH/SD) in-plane	948	902	11.5	22.4	911m	910m	916mbr	914m	$100S_{21}$	703	683	659m	660sh	$85S_{21}$
ν_{22}	δ_{wag}(CH)	875	874	5.7	0.4	969w	970vw	970sh	973w	$64S_{22}$ $18S_{23}$ $12S_{27}$	875	868	976m	–	$61S_{22}$ $25S_{23}$ $10S_{27}$
ν_{23}	δ_{wag}(CH)	865	864	2.9	2.5	963w	940w	–	940sh	$63S_{23}$ $31S_{27}$	865	865	935s	936w	$58S_{23}$ $41S_{27}$
ν_{24}	Ring breathing	859	840	10.4	8.4	850m	–	–	–	$15S_{24}$ $19S_{35}$ $13S_{20}$ $12S_{15}$	836	818	849s	–	$13S_{24}$ $28S_{35}$ $20S_{15}$ $14S_{20}$
ν_{25}	δ_{wag}(CH)	806	805	2.4	4.9	832m	838s	835wbr	–	$72S_{25}$ $18S_{22}$ $12S_{27}$	805	805	814s	814w	$59S_{25}$ $20S_{26}$ $14S_{28}$ $11S_{23}$
ν_{26}	$\delta_{wag}(NH_2/ND_2)$	765	747	309.9	7.5	749s	754w	750vs	758w	$42S_{26}$ $18S_8$	620	596	659m	660sh	$42S_{26}$ $27S_{28}$ $14S_{25}$
ν_{27}	δ_{wag}(CH)	730	714	69.4	4.9	710w	718vw	–	705sh	$28S_{27}$ $18S_{23}$ $18S_{22}$ $14S_{26}$ $12S_{25}$	747	744	–	712w	$34S_{27}$ $22S_{16}$
ν_{28}	υ(C–S)	699	687	6.0	8.4	677m	680s	676m	680s	$22S_{28}$ $26S_{29}$ $16S_{35}$ $11S_{20}$ $11S_{32}$	696	672	676m	676m	$35S_{28}$ $29S_{23}$ $19S_{26}$ $10S_{25}$
ν_{29}	δ_{ring}(CCC)	569	561	1.6	7.6	534m	564m	–	564s	$41S_{29}$ $18S_{35}$ $10S_{15}$	560	551	–	554w	$62S_{29}$ $13S_{22}$
ν_{30}	NH_2/ND_2 torsion	520	519	19.4	1.3	–	542w	526	541	$70S_{30}$ $20S_{39}$	443	443	–	(433w)	$60S_{30}$ $35S_{33}$
ν_{31}	δ(CCN)	478	475	2.6	4.8	–	484s	468m	475s	$52S_{31}$ $16S_{28}$ $10S_{24}$	453	449	–	(433w)	$21S_{31}$ $24S_{23}$
ν_{32}	δ_{ring}(CCC)	444	444	1.7	0.3	–	–	–	(439m)	$60S_{32}$ $10S_{30}$	493	486	–	482w	$45S_{32}$ $18S_{39}$ $15S_{26}$
ν_{33}	Ring puckering	420	419	8.2	0.8	–	–	–	(439m)	$80S_{33}$ $18S_{39}$	412	411	–	(433w)	$40S_{33}$ $15S_{39}$ $30S_{38}$ $10S_{24}$
ν_{34}	SH/SD torsion	395	374	23.5	2.1	–	374s	–	373s	$29S_{34}$ $20S_{37}$ $20S_{34}$	289	263	–	(252vw)	$39S_{34}$ $26S_{32}$ $14S_{38}$
ν_{35}	δ_{ring}(CCC)	376	344	0.3	2.0	–	–	–	311w	$21S_{35}$ $25S_{31}$ $24S_{28}$ $11S_{17}$	364	362	–	366vw	$34S_{35}$ $30S_{28}$ $14S_{32}$ $11S_{39}$
ν_{36}	Ring puckering	266	263	2.8	1.2	–	(262m)	–	(260m)	$35S_{36}$ $10S_{33}$ $10S_{31}$	251	245	–	(252vw)	$35S_{36}$ $10S_{33}$ $10S_{31}$
ν_{37}	Ring puckering	239	237	7.3	1.8	–	(262m)	–	(260m)	$42S_{37}$ $20S_{34}$ $20S_{31}$	126	125	–	–	$42S_{37}$ $20S_{34}25S_{31}$ $15S_{39}$
ν_{38}	Ring puckering	183	166	16.2	2.2	–	(170s)	–	(172s)	$50S_{38}$ $26S_{31}$	153	152	–	166wm	$40S_{38}$ $10S_{31}$
ν_{39}	δ_{wag}(C–S)	148	143	3.9	5.0	–	(170s)	–	(172s)	$33S_{39}$ $30S_{38}$ 20 S_{34}	226	219	–	–	$18S_{39}$ $26S_{38}$ $14S_{26}$

[a] Unscaled *ab initio* wavenumbers from MP2/6-31G(d) basis set.
[b] Fixed scaling factors of 0.95 have been used for υ(CH), υ(CC), δ(CH), δ(CC), δ(HCC) and δ(HNH) modes, 0.9 for υ(SH), υ(NH), δ(SOC) and δ(HNC). But 1.0 scaling factor is used for υ(CN), υ(CS), δ_{wag}(CN), δ_{wag}(CS), δ(NCC), δ(CCS), $\delta_{wag}(NH_2)$ and τ(CCCC) (ring puckering).
[c] Calculated Raman activities in $Å^4$/amu at MP2/6-31G(d) basis set.
[d] Calculated infrared intensities in kcal/mol at MP2/6-31G(d) basis set.
[e] Observed bands marked with asterisks are from IR and/or R spectra of the solid. Bands between brackets are used for two fundamentals modes.
[f] Contributions less than 10% are omitted.

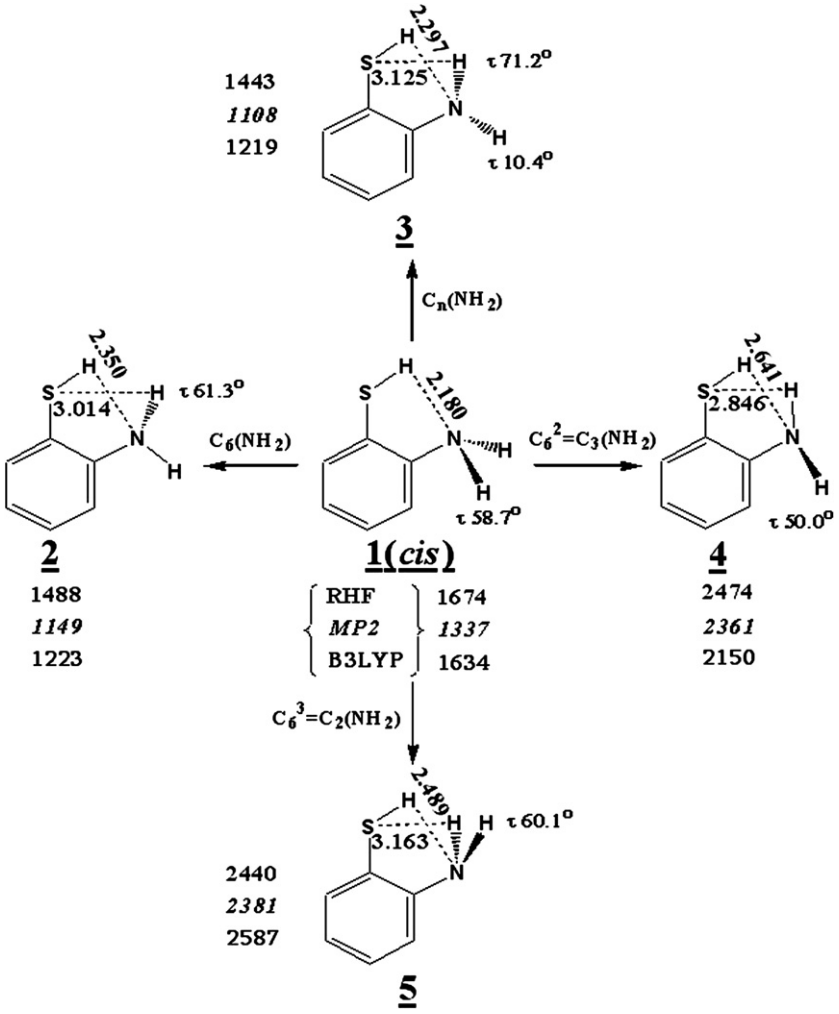

Fig. 3. Conformational isomerism of 2-aminothiophenol, where the SH group is directed towards the NH_2 moiety, the energy differences (ΔE) between all isomers and **11** (*gauche-2*) is given in cm^{-1}.

516 cm^{-1} (1.47 kcal/mol). After that, the energy decreases when τ_1 is larger than 60° till reaching a *unique minimum* conformation (**11**) named *gauche-2* at τ_1 of 129.4° which is equivalent to HSC_1C_3 dihedral angle of 51.6° ($E = -683.28343$ Hartree). For *gauche-2* (**11**) conformer the NH_2 group is ⊥ to the benzene ring while the out-of-plane (oop) SH is directed towards NH_2 and the lone pair(s) on nitrogen and sulfur atoms resides in opposite directions. When τ_1 is larger than 130°, the energy reaches another maximum (conformer **3**), the SH barrier (V_2) of 2491 cm^{-1} (7.12 kcal/mol) is estimated between (**11**) and (**3**) conformers (Table 4 and Fig. 6).

In view of the abovementioned PSS, we allowed complete relaxation of all geometrical parameters of the new (*gauche-2*; **11**) minimum starting with dihedral angles of 43.0° for $H_{15}N_4C_3C_1$, 12.1° for $H_{14}N_4C_3C_5$ and 130° for HSC_1C_{11} employing MP2/6-31G(d) calculations. The optimized MP2/6-31G(d) SPs of *gauche-2* isomer are listed in Table 2 and the aforesaid torsion angles are found to be 34.6°, 19.0° and 128.4°, respectively. Accordingly, we carried out an extra PSS employing SPs (Table 2) of *gauche-2* (**11**) conformer; the PSS energies are expressed in both cm^{-1} and kcal/mol as seen in Table 4 and Fig. 6, the SH barriers are ranged from 3 to 6 kcal/mol compared to 1.34, 1.79 and 2.46 kcal were recorded by the National Institute of Standards and Technology (NIST) for CH_3SH, CH_3CH_2SH and $HSCH_2CH_2SH$, respectively.

For 2AP, we did not observe a convergence minimum in the vein of *gauche-2* (**11**) isomer [19], therefore we rotated the OH group around C–O bond implementing MP2/6-31G(d) optimized SPs to check the existence of conformer (**11**). Contrary to 2ATP, the PSS results definitely exclude *gauche-2* (**11**) in 2AP molecule (Table 4 and Fig. 6) and the *trans* (**8**) isomer still a minimum. The energy increases upon rotating the OH group till $\tau_1 = 90°$ (884 cm^{-1}) then decreases a little bit (±6.98 cm^{-1}) followed by further increase at 120° (908 cm^{-1}) followed by another maximum at 180° (3825 cm^{-1}). The little energy hump around 90° (±6.98 cm^{-1}) was not visible in Fig. 6 due to the large *Y* axis scale. The numbers between brackets represent the barriers between *trans* (**8**) ($\tau_1 = 0°$) and other high energy structures at dihedral angles of 90°, 120° and 180°, respectively.

To compare and evaluate the size and electronegativity effects on OH and SH barriers to internal rotation we have performed PSS for phenol (C_6H_5OH) and thiophenol (C_6H_5SH) using optimized SPs from MP2/6-31G(d) calculations. The planar phenol was found to be minimum with an OH barrier of 1157 cm^{-1} (3.31 kcal/mol); OH ⊥ to the benzene ring. This barrier complements well with an OH barrier of 1213 (3.47 kcal/mol) and 1007 cm^{-1} (2.88 kcal/mol) obtained from the far-IR spectrum of gaseous phenol and *p*-fluorophenol, respectively [28]. On the other hand, the thiophenol minimum is fluctuating in the vicinity of 30° (CCSH torsion angle), i.e., thiophenol is non-planar. The energy difference between planar and non-planar thiophenol is margined only by 4–24 cm^{-1} (τ varies from 0° to 40°) which reflects relatively coincident energies

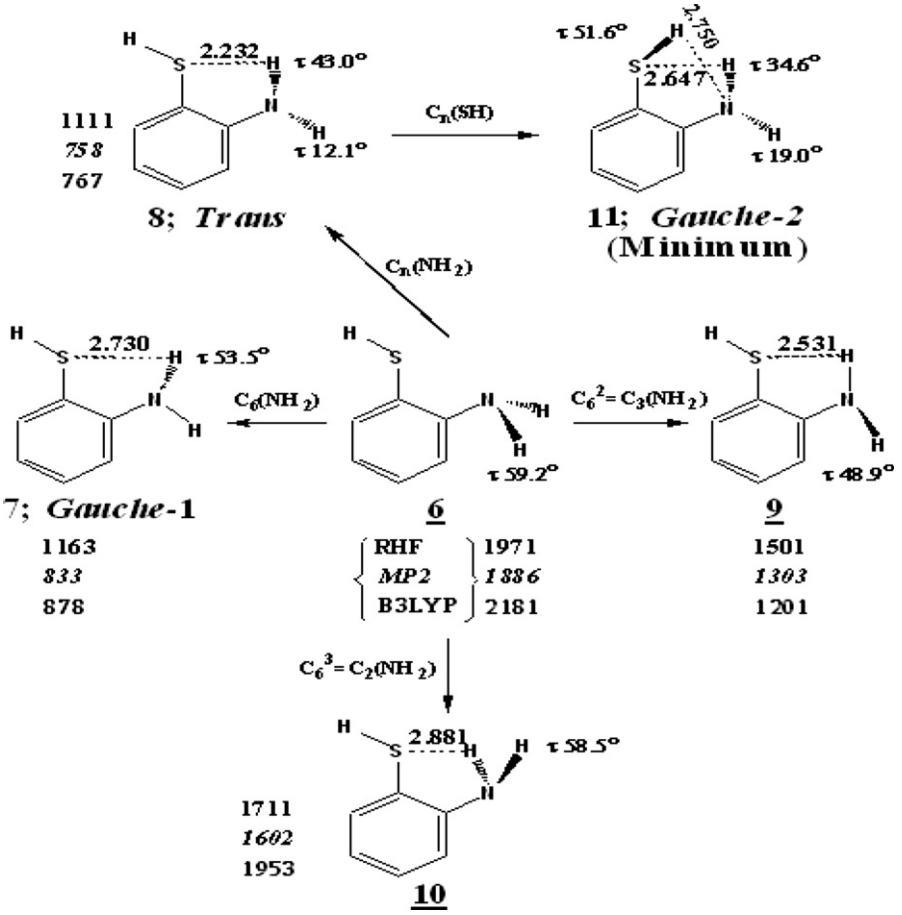

Fig. 4. Conformational isomerism of 2-aminothiophenol, where the SH group is directed away from the NH_2 moiety, the energy differences (ΔE) between all isomers and **11** (*gauche-2*) is given in cm^{-1}.

of these conformations. The calculated SH barrier (V_2) between conformers (**11**) and (**8**) was 1194 cm^{-1} in close proximity to that given earlier [28], see Table 4 and Fig. 7.

For the C–NH_2 moiety, an increase of C–N bond length favors SP^3 hybridization whereas the shortening of the C–N bond length favors SP^2 hybridization [29]. The possibility of planar NH_2 is ignored, due to the calculation of two imaginary wavenumbers and high energies as well. The NH_2 barriers to internal rotation were calculated using the MP2/6-31G(d) optimized SPs for 2AP (*trans* **8**) and 2ATP (*gauche* **11**). For *trans* (**8**) 2AP, the OH is in-plane and away from NH_2 group [19], however the SH moiety is out-of-plane towards NH_2 in case of *gauche-2* (**11**) conformer. The NH_2 moiety rotates around C–N bond by 10° increments of $H_{15}N_4C_3C_1$ dihedral angle, the PSS results are summarized in Table 4 and Fig. 8. The NH_2 barriers are symmetric in case of 2AP (C_s symmetry) but asymmetric in case of 2ATP owing to out-of-plane SH moiety (C_1 symmetry).

The predicted NH_2 barriers of 2ATP are about one third to that obtained for 2AP which is attributed to the lengthening of C–S bond that minimizes the lone pair–lone pair interactions in 2ATP. For that reason, the SH barriers are also lower than that of OH barriers (Table 4). In addition, the relatively high SH barriers of 3–6 kcal/mol (Fig. 6) and high NH_2 barriers of 3–9 kcal/mol of 2ATP, allow us to focus on the vibrational assignment of conformer **11**. From earlier investigations [30,31], NH_2 barriers varies from 1.0 kcal/mol (vinylamine; MW), 2.03 ± 0.01 kcal/mol ($CH_3CH_2NH_2$; R), 1.6 kcal/mol ($CH_2{=}CH{-}NH_2$), 2.3 and 3.3 kcal/mol ($O{=}C{=}CH{-}NH_2$; B3LYP/6-311+G** and MP2/6-311+G**). Moreover, barriers of 2.39, 3.80 and 10.99 kcal/mol have been recorded by the National Institute of Standards and Technology (NIST) for CH_3NH_2, $C_6H_5NH_2$ and CH_3CONH_2, respectively. These differences in NH_2 barriers are devoted to either weak or strong hydrogen bonding interactions along with lone pair and steric interactions. Eventually, all computational calculations were carried out using Toshiba (1.7 GHz), and/or Acer (2.93 GHz), 512–1056 MB memory. The proposed structures of 2ATP were visualized and recognized using an interactive shareware molecular graphics program called MOLEKEL 4.0 [32].

4. Normal coordinate analysis

To carry out normal coordinate analysis, a similar method to symmetry adopted linear combination [33] was exploited to express all vibrational motions of 2ATP in terms of chosen internal coordinates. Similar to 2AP, 45 independent internal coordinates (Fig. 5) have been used to form 39 symmetry coordinates (Table 5) using the traditional method of Wilson [34]. For C_1 symmetry, all vibrational modes are both infrared and Raman active and expected to be polarized.

The following method was used to transform *ab initio* results into the form required for iterative normal coordinate program. The output files of QM calculations contain the FCs in Cartesian coordinates in Hartree/$Bohr^2$ units. These FCs must be transformed into internal coordinates using mdyne/Å unit for stretch–stretch, stretch–bend and bend–bend interactions. The Cartesian coordinates were introduced into G-matrix program, and then the calculated B-matrix was used to convert the unscaled *ab initio* force fields in Cartesian coordinates to a force field in the chosen internal coordinates. The scaled diagonal FCs and the scaling factors together with the definition of internal coordinates for *gauche-1*,

Table 2
MP2 and X-ray structural parameters[a] for *gauche-2* (**11**) and *trans* (**8**) 2-aminothiophenol utilizing 6-31G(d), 6-311+G(d) and 6-31++G(d,p) basis sets

Parameters	X-ray Ref. [42]	MP2 for *gauche-2* (**11**)			MP2 for *trans* (**8**)		
		6-31G(d)	6-311+G(d)	6-31++G(d,p)	6-31G(d)	6-311+G(d)	6-31++G(d,p)
$r(S_2H_{13})$		1.344	1.349	1.335	1.340	1.344	1.330
$r(N_4H_{14})$		1.015	1.010	1.010	1.016	1.010	1.010
$r(N_4H_{15})$		1.017	1.012	1.012	1.017	1.012	1.012
$r(C_1S_2)$	1.747(1)	1.783	1.778	1.780	1.778	1.771	1.773
$r(C_3N_4)$	1.370(1)	1.401	1.397	1.399	1.406	1.402	1.403
$r(C_1C_3)$	1.425(2)	1.409	1.411	1.409	1.409	1.410	1.408
$r(C_3C_5)$	1.410(2)	1.403	1.404	1.402	1.401	1.403	1.401
$r(C_5C_7)$	1.389(2)	1.392	1.395	1.393	1.393	1.395	1.393
$r(C_7C_9)$	1.400(2)	1.396	1.399	1.397	1.395	1.398	1.396
$r(C_9C_{11})$	1.388(2)	1.394	1.96	1.394	1.395	1.396	1.394
$r(C_{11}C_1)$	1.398(2)	1.398	1.400	1.399	1.398	1.401	1.399
$r(C_5H_6)$		1.089	1.089	1.084	1.089	1.089	1.084
$r(C_7H_8)$		1.087	1.087	1.082	1.087	1.087	1.082
$r(C_9H_{10})$		1.087	1.086	1.081	1.087	1.086	1.082
$r(C_{11}H_{12})$		1.087	1.087	1.082	1.088	1.088	1.083
$r(S_2....H_{14})$		4.026[b]	4.028[b]	4.021[b]	3.948[b]	3.943[b]	3.944[b]
$r(S_2....H_{15})$		2.647[c]	2.656[c]	2.642[c]	2.632[c]	2.598[c]	2.598[c]
$r(S_2....H_{12})$		2.856[c]	2.853[c]	2.859[c]	2.952[c]	2.950[c]	2.945[c]
$\angle(C_1S_2H_{13})$		96.1	95.6	95.6	95.5	95.7	95.4
$\angle(S_2C_1C_{11})$		119.2	119.2	119.4	122.9	122.9	122.8
$\angle(S_2C_1C_3)$		120.8	120.7	120.6	117.4	117.4	117.6
$\angle(N_4C_3C_1)$		120.3	120.4	120.4	119.7	120.3	120.1
$\angle(N_4C_3C_5)$		121.1	121.1	120.8	121.3	121.0	120.9
$\angle(C_3C_1C_{11})$		120.1	120.1	119.9	119.7	119.7	119.6
$\angle(C_1C_3C_5)$		118.6	118.5	118.7	118.9	118.8	119.0
$\angle(C_3C_5C_7)$		120.9	121.1	121.0	121.1	121.3	121.1
$\angle(C_5C_7C_9)$		120.2	120.1	120.2	119.8	119.8	119.8
$\angle(C_7C_9C_{11})$		119.4	119.3	119.4	119.6	119.6	119.6
$\angle(C_1C_{11}C_9)$		120.8	120.8	120.8	120.8	120.9	120.9
$\angle(C_3N_4H_{14})$		112.9	113.9	113.9	112.5	113.4	113.4
$\angle(C_3N_4H_{15})$		112.7	113.8	113.8	113.4	114.5	114.5
$\angle(H_{14}N_4H_{15})$		110.7	111.7	111.6	109.5	110.5	110.2
$\angle(C_1C_{11}H_{12})$		118.8	118.7	118.8	119.5	119.6	119.5
$\angle(C_9C_{11}H_{12})$		120.4	120.5	120.4	119.6	119.5	119.6
$\angle(C_{11}C_9H_{10})$		120.0	120.1	120.0	119.7	119.8	119.8
$\angle(C_7C_9H_{10})$		120.6	120.6	120.6	120.6	120.7	120.6
$\angle(C_9C_7H_8)$		120.3	120.4	120.3	120.4	120.5	120.5
$\angle(C_5C_7H_8)$		119.5	119.5	119.5	119.7	119.7	119.7
$\angle(C_7C_5H_6)$		120.0	119.8	120.0	120.1	119.9	120.1
$\angle(C_3C_5H_6)$		119.0	119.1	119.0	118.9	118.9	118.8
$\tau(C_1C_3N_4H_{15})$		34.6	34.1	32.9	43.0	37.3	37.3
$\tau(C_1C_3N_4H_{14})$		19.0	16.3	17.7	12.1	14.6	15.0
$\tau(C_3C_1S_2H_{13})$		51.6	53.3	53.9	180.0	180.0	180.0
A, MHz		2914	2910	2920	2944	2937	2943
B, MHz		1535	1535	1535	1536	1538	1539
C, MHz		1011	1011	1012	1011	1011	1012
μ_{tot}, Debye		1.849	1.845	1.792	1.750	1.471	1.490

[a] Bond distances in Å, bond and dihedral angles in degrees, rotational constants *A*, *B*, *C* in MHz and total dipole moment (μ_{tot}) in Debye.
[b] S....H bond distance does not represent intramolecular hydrogen bonding.
[c] Intramolecular hydrogen bonding.

Table 3
RHF, MP2 and B3LYP energies in Hartree for **11**, **8** and **7** conformers of 2-aminothiophenol

	Gauche-2; **11**	*Trans*; **8**	*Gauche-1*; **7**	ΔE_1[b], cm^{-1}	ΔE_2[c], cm^{-1}
At 6-31G(d) basis set					
RHF level	−683.2403103	−683.2352500	−683.2350107	1111	833
MP2 level	−684.2845352	−684.2810837	−684.2807413	758	1163
B3LYP level	−685.7898725	−685.7863764	−685.7858723	767	878
At 6-311+G(d) basis set					
RHF level	−683.3213754	−683.316214	−683.3161057	1087	1156
MP2[a] level	−684.6791318	−684.6751681	−684.6746498	870	984
B3LYP level	−685.8860626	−685.8825526	−685.8820607	770	879
At 6-31++G(d,p) basis set					
RHF level	−683.2693615	−683.2642232	−683.2638363	1565	1213
MP2[a] level	−684.4181583	−684.4137911	−684.4132839	958	1261
B3LYP level	−685.8208705	−685.8173351	−685.8167777	776	898

[a] MP2 calculations have been carried out with full electron correlation.
[b] ΔE_1 represents the energy difference between *gauche-2* (minimum energy, **11**) and *trans* isomer (**8**).
[c] ΔE_2 represents the energy difference between *gauche-2* and *gauche-1* isomer (**7**).

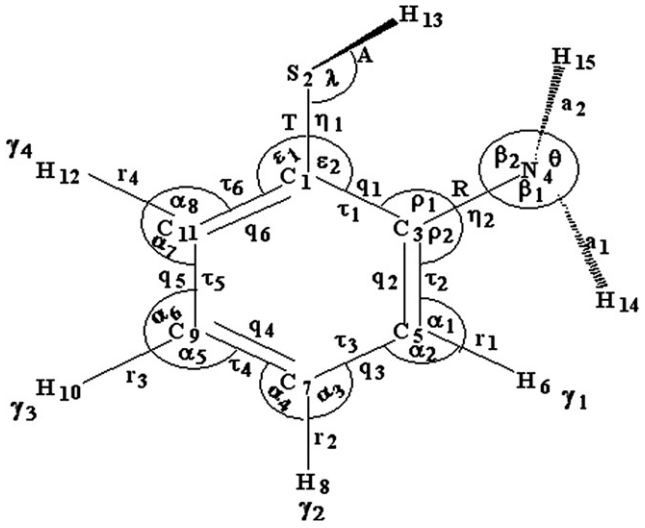

Fig. 5. Internal coordinates definitions of the stable *gauche-2* conformer of *ortho*-aminothiophenol where $NH_2 \perp$ benzene ($HSC_1C_3 = 51.6°$) and SH is out-of-plane ($H_{15}NC_3C_1 = 34.6°$).

gauche-2 and *trans* 2ATP compared with fully converged structures of 2AP [19] are listed in Table 6. All the diagonal elements of FCs have been assigned scaling factors into a force constant program developed by Durig's group at the UMKC which is similar to that written by Schachtschneider [35]. Initially, all scaling factors have been kept fixed at a value of 1.0 to produce the pure *ab initio* calculated frequencies. Then, rational scaling factors were used to obtain the fixed scaled quantum mechanical molecular force field to evaluate theoretical wavenumbers against experimental values [36–39]. These scaling factors are essential to compensate for systematic errors such as basis set defects, electron correlation and neglecting of anharmonic effect [36–39]. Consequently, scaling factors of 0.95 have been used for υ(CH), υ(CC), δ(CH), δ(CC), δ(HCC) and δ(HNH) modes, 0.9 for υ(SH), υ(NH), δ(SOC) and δ(HNC). But 1.0 scaling factor is used for υ(CN), υ(CS), δ_{wag}(CN), δ_{wag}(CS), δ(NCC), δ(CCS), $\delta_{wag}(NH_2)$ and τ(CCCC) (ring puckering). Either SH or NH_2 torsion mode will break the existing intramolecular hydrogen bonding; therefore a scaling factor of 0.75 was used for these fundamentals. With this program we calculated the matrices of potential energy distributions (PEDs) for the minimum *gauche-2* conformers which provide a measure of each internal coordinate contribution to the normal coordinate (Table 1). The computational results using B3LYP/6-31G(d) basis set for *gauche-2* and *trans* (**8**) are listed in Supplementary Table B. In addition the calculated MP2/6-31G(d) wavenumbers and PEDs for *trans* (**8**) are produced in Supplementary Table C.

5. Structural parameters and force constants

The sum of van der Waal contact radii for sulfur and hydrogen atoms (S····H) is about 3.0 Å [40,41] and the calculated S····H bond length ranged from 2.65 to 2.73 Å for *gauche-2*, *gauche-1* and *trans* conformers. These distances favor intramolecular hydrogen bonding between sulfur and hydrogen atoms. Likewise, the calculated N····H distance of 2.750 Å for *gauche-2* conformer is similar to the sum of van der Wall radii (~2.75 Å) for nitrogen and hydrogen atoms [40,41]. In contrast, the O····H and N····H bond lengths are less than van der Waal radii by ~0.3 Å, thus 2ATP is expected to have less intramolecular hydrogen bonding interactions compared to 2AP. However, the possibility of intramoleculer (N····H) hydrogen bonding vanishes for *gauche-1* (**7**) and *trans* (**8**) isomers because the SH group is away from NH_2 moiety.

It is interesting that the calculated C–S, C–N bond lengths for *gauche-1*, *gauche-2* and *trans* isomers (Table 2) are in agreement within ±0.01–0.02 Å to X-ray values [42]. From X-ray crystallographic data of 2ATP Ni and Co complexes, values of

Table 4
Barriers[a] to internal rotations for *trans* (**8**) and *gauche-2* (**11**) conformers of 2-aminothiophenol (2ATP), *trans* (**8**) conformer of 2-aminophenol (2AP) and *cis* (**1**) compared with phenol and thiophenol

Dihedral angle (τ°)	($NH_2C_6H_5SH$) *Trans* (**8**)[b]		($NH_2C_6H_5SH$) *Gauche-2* (**11**)[b]		($NH_2C_6H_5OH$) *Trans* (**8**)[b]		($NH_2C_6H_5SH$) *Gauche-2* (**11**)[c]		($NH_2C_6H_5OH$) *Cis* (**1**)[c]		Phenol (C_6H_5OH)[d]		Thiophenol (C_6H_5SH)[d]	
	Energy (kcal/mole)	Energy (cm^{-1})	Energy (kcal/mole)	Energy (cm^{-1})	Energy (kcal/mole)	Energy (cm^{-1})	Energy (kcal/mole)	Energy (cm^{-1})	Energy (kcal/mole)	Energy (cm^{-1})	Energy (kcal/mole)	Energy (cm^{-1})	Energy (kcal/mole)	Energy (cm^{-1})
0	1.47	516	2.82	988	0.00	0	7.88	2757	0.00	0	0.00	0	0.03	11
10	1.94	678	3.02	1056	0.13	46	7.34	2567	0.09	31	0.12	42	0.02	7
20	2.39	836	3.39	1185	0.41	145	6.37	2228	0.63	127	0.46	160	0.01	2
30	2.75	963	3.44	1204	0.83	291	5.13	1793	0.85	296	0.99	345	0.00	0
40	2.99	1045	3.35	1170	1.24	435	3.74	1310	1.59	555	2.36	575	0.03	11
50	3.06	1069	3.10	1084	1.67	586	2.40	841	2.63	920	2.35	823	0.09	28
60	2.95	1032	2.73	955	2.04	715	1.24	434	4.05	1418	3.04	1064	0.21	75
70	2.68	937	2.27	794	2.27	794	0.40	140	5.96	2083	3.63	1269	0.33	116
80	2.28	797	1.78	621	2.47	865	0.00	0	8.39	2936	4.05	1418	0.45	158
90	1.80	630	1.28	446	2.53	884	0.13	46	11.33	3962	4.28	1479	0.54	189
100	1.28	446	0.80	281	2.51	877	0.80	280	14.48	5063	4.77	1503	0.59	208
110	0.75	261	0.39	136	2.49	873	1.96	685	17.15	5998	4.11	1438	0.61	215
120	0.28	99	0.09	33	2.60	908	3.42	1198	18.38	6430	3.74	1317	0.62	217
130	0.0	0.0	0.0	0.0	2.97	1038	4.98	1740	17.68	6185	3.31	1157	0.64	226
140	0.09	32	0.56	197	3.78	1321	6.33	2214	15.68	5485	2.81	985	0.71	248
150	0.82	288	1.10	384	5.15	1800	7.27	2543	13.38	4681	2.36	827	0.81	283
160	2.39	836	2.58	902	7.04	2463	7.76	2715	11.46	4008	2.01	702	0.93	325
170	4.71	1648	4.54	1589	9.16	3204	7.79	2726	10.21	3573	1.78	621	1.04	364
180	7.12	2491	6.41	2241	10.94	3825	7.49	2620	9.80	3428	1.70	595	1.09	380

[a] Barriers are obtained from potential surface scan at MP2/6-31G(d) basis set.
[b] See Fig. 6.
[c] See Fig. 8.
[d] See Fig. 7.

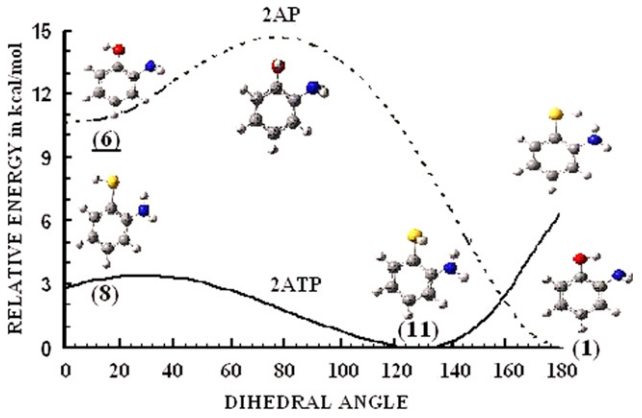

Fig. 6. OH and SH barriers to internal rotation using MP2/631G(d) optimized parameters of *trans* (**6**) 2-aminophenol (2AP) and *trans* (**8**) 2-aminothiophenol, respectively.

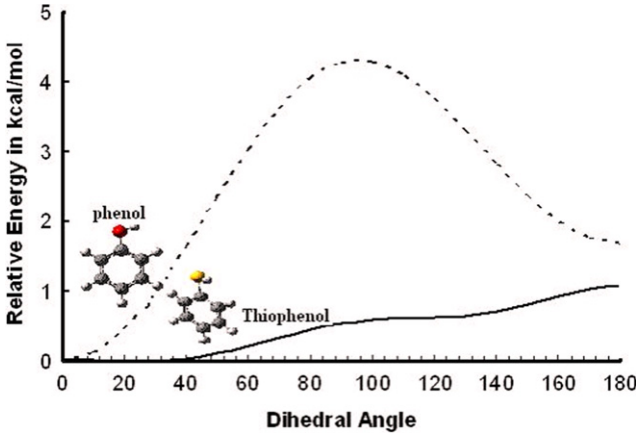

Fig. 7. OH and SH barriers to internal rotation using MP2/631G(d) optimized parameters of phenol and thiophenol, respectively.

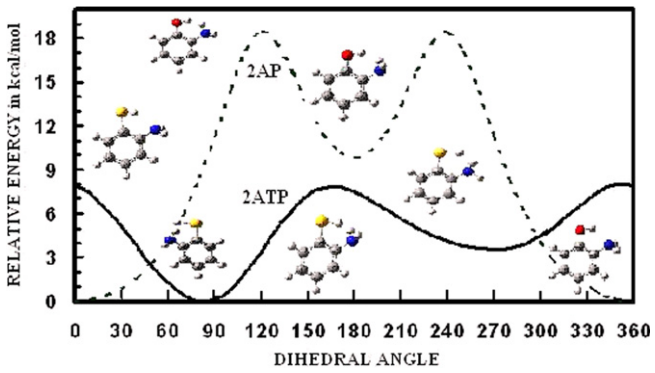

Fig. 8. NH_2 barriers to internal rotation using MP2/631G(d) optimized parameters *cis* (**1**) 2-aminophenol (2AP) and *gauche-2* (**11**) of 2-aminothiophenol.

1.747 ± 0.004 (C–S) and 1.371 ± 0.005 Å (C–N) are reported which are between single and double bond lengths. Similarly the calculated C–C bond length is characteristic for phenyl ring which suggests a bond order of 1.5 for C–C, along with C–S and C–N bonds.

Utilizing MP2 and B3LYP calculations at the same basis for 2ATP (Table 2 and Supplementary Table A), the C–S and C–N bond lengths vary only by 0.01–0.001 Å and the NCC angle varies only by ±0.1° which is similar to those achieved for 2AP (C–S, C–N the NCC) [19]. The calculated $C_1C_3C_5$ angle is found to be 118.6(1)° and 120.5(5)° for 2ATP and 2AP, respectively, where C_3 is attached to nitrogen atom. These values are comparable to the 121.6(2)° obtained from electron diffraction (ED) of *p*-bromonitrobenzene [42]. The angular distortion of the benzene ring and the electronegativity of the subsistent groups are expected to affect the CCC internal angle [43], however the $C_3C_1C_{11}$ angle in 2AP [19] and 2ATP differs only by 0.1–0.2° with and without polarization and diffusion functions. The calculated torsion angles of $C_1C_3N_4H_{14}$ from MP2 level are larger than those predicted from B3LYP by ~1–5°, but a variation of 9–14° is calculated for $C_1C_3N_4H_{14}$ and $C_3C_1S_2H_{13}$. Finally, the calculated rotational constants, *A*, *B* and *C* from MP2 level and B3LYP do not differ significantly; they vary by 6–11 MHz (Table 2 and Supplementary Table A). No significant change in the optimized SPs occur with the addition of diffuse functions (6-31+G**) and the triple split valence basis set (6-311G**) for the non-hydrogen atoms.

The force constants (FCs) for lower energy conformations of 2AP and 2ATP are listed together in Table 6. For *gauche-1*, *gauche-2* and *trans* isomers, the calculated stretching and bending FCs vary by 0.1–0.2 and 0.02–0.002 mdyne/Å, respectively. The lowest energy conformer *gauche-2* is distinctive for 2ATP only, thus its FCs are not compared with 2AP analogue. On the other hand, B3LYP frequency calculations predicts an imaginary torsion frequency for 2AP *gauche-1* (**7**), thus its FCs are not listed in Table 6. For the SH and OH in-plane, the CSH and COH bending FCs diverge by ~8%. Differences of ~40% between B3LYP and MP2 FCs for CX and XH (X = O or S) stretches of 2AP and 2ATP molecules are reported.

6. Simulated infrared and Raman spectra

It has already been established that, a clear prediction of Raman (R) and infrared (IR) spectra is essential in vibrational analysis of organic molecules making vibrational spectroscopy a more practical tool [44–46]. The dipole moments, polarizability derivatives as well as frequencies have been extracted from G98 output file to produce the simulated vibrational spectra of *gauche-2* (**11**) and *trans* (**8**) 2ATP (Fig. 9). The Raman spectrum is simulated using the calculated Raman scattering activities from MP2 (Tables 1 and Supplementary Table C). The Raman scattering cross section is proportional to the Raman intensity which can be calculated from the scattering activities and the predicted frequencies for each normal mode [47–50]. The simulated IR spectra of of *gauche-2* (**11**) and *trans* (**8**) conformers were calculated based on infrared intensities and dipole moment derivatives with respect to the Cartesian coordinates. The derivatives were taken from the *ab initio* calculations then transformed to the normal coordinates. Detailed description of the entire procedure are given elsewhere [51], the simulated spectra utilizing B3LYP/6-31G(d) calculations are available on request.

7. Vibrational assignments and discussion

The vibrational assignments of aminothiophenol derivatives [11,12,17] neglect hypothetical rotational isomerism based on *cis* (**1**) and *trans* (**8**) conformations, where the N–H bonds are not eclipsing the benzene ring and the SH group is directed towards the NH_2 group. Moreover, two extra *gauche* conformations have been verified (**11** and **7**) besides the above mentioned *trans* (**8**). From MP2/6-31G(d) basis set, the *gauche-2* (**11**) isomer is more stable than *trans* and *gauche-1* (**7**) by 758 and 833 cm^{-1}, respectively, with real frequencies (Fig. 4 and Table 3). On the other hand, a negative ring torsion frequency is estimated for *cis* (**1**) which is energetically higher than *gauche-2* (**11**) by 1674, 1337 and

Table 5
Symmetry coordinates[a] for 2-aminothiophenol ($-d_0$ and d_3)

Species	ν_i[b]	Definition	Symmetry coordinate
A″	ν_1	NH_2/ND_2 antisymmetric stretch.	$S_1 = a_1 - a_2$
A′	ν_2	SH/SD symmetric stretch	$S_2 = A$
A′	ν_3	NH_2/ND_2 symmetric stretch	$S_3 = a_1 + a_2$
A′	ν_4	CH symmetric stretch	$S_4 = r_1 + r_2 + r_3 + r_4$
A′	ν_5	CH symmetric stretch	$S_5 = r_1 - r_2 - r_3 + r_4$
A′	ν_6	CH antisymmetric stretch	$S_6 = r_1 + r_2 - r_3 - r_4$
A′	ν_7	CH antisymmetric stretch	$S_7 = r_1 - r_2 + r_3 - r_4$
A′	ν_8	NH_2/ND_2 scissors	$S_8 = \theta$
A′	ν_9	CC ring stretch	$S_9 = q_3 - q_5 - q_4 + q_6$
A′	ν_{10}	CC ring stretch	$S_{10} = 2q_1 - q_3 - q_5 - 2q_2 + q_4 + q_6$
A′	ν_{11}	CH in-plane deformation	$S_{11} = \alpha_1 - \alpha_2 - \alpha_7 + \alpha_8$
A′	ν_{12}	CH in-plane deformation	$S_{12} = \alpha_3 - \alpha_4 + \alpha_5 - \alpha_6$
A′	ν_{13}	CC ring stretch	$S_{13} = q_1 + q_3 + q_5 - q_2 - q_4 - q_6$
A′	ν_{14}	SH/SD in-plane deformation	$S_{14} = \lambda$
A′	ν_{15}	C–S stretch	$S_{15} = T$
A′	ν_{16}	C–N stretch	$S_{16} = R$
A′	ν_{17}	CH in-plane deformation	$S_{17} = \alpha_1 - \alpha_2 + \alpha_7 - \alpha_8$
A″	ν_{18}	NH_2/ND_2 twist	$S_{18} = \beta_1 - \beta_2$
A′	ν_{19}	CH in-plane deformation	$S_{19} = \alpha_3 - \alpha_4 - \alpha_5 + \alpha_6$
A′	ν_{20}	CC ring stretch	$S_{20} = q_3 - q_5 + q_4 - q_6$
A′	ν_{21}	CC ring stretch	$S_{21} = 2q_1 - q_3 - q_5 + 2q_2 - q_4 - q_6$
A′	ν_{22}	NH_2/ND_2 wag	$S_{22} = \beta_1 + \beta_2$
A″	ν_{23}	CH wag	$S_{23} = \gamma_1 + \gamma_2 - \gamma_3 - \gamma_4$
A′	ν_{24}	CCC in-plane deformation	$S_{24} = \alpha_1 + \alpha_2 - \alpha_7 - \alpha_8$
A″	ν_{25}	CH wag	$S_{25} = \gamma_1 - \gamma_2 + \gamma_3 - \gamma_4$
A″	ν_{26}	CH wag	$S_{26} = \gamma_1 - \gamma_2 - \gamma_3 + \gamma_4$
A′	ν_{27}	CC ring breathing	$S_{27} = q_1 + q_2 + q_3 + q_4 + q_5 + q_6$
A″	ν_{28}	CH wag	$S_{28} = \gamma_1 + \gamma_2 + \gamma_3 + \gamma_4$
A″	ν_{29}	SH/SD torsion	$S_{29} = \eta_1$
A′	ν_{30}	CCC ring in-plane deformation	$S_{30} = \alpha_1 + \alpha_2 + \alpha_7 + \alpha_8$
A′	ν_{31}	CCC ring in-plane deformation	$S_{31} = \alpha_3 + \alpha_4 + \alpha_5 + \alpha_6$
A″	ν_{32}	C–S wag	$S_{32} = \gamma_5$
A′	ν_{33}	CCC ring in-plane deformation	$S_{33} = \alpha_3 + \alpha_4 - \alpha_5 - \alpha_6$
A″	ν_{34}	CCCC ring puckering (τ(CC))	$S_{34} = 2\tau_1 - \tau_3 - \tau_5 - 2\tau_2 + \tau_4 + \tau_6$
A″	ν_{35}	CCCC ring puckering (τ(CC))	$S_{35} = \tau_3 - \tau_5 - \tau_4 + \tau_6$
A′	ν_{36}	CCN in-plane deformation	$S_{36} = \rho_1 - \rho_2$
A″	ν_{37}	NH_2/ND_2 torsion	$S_{37} = \eta_2$
A″	ν_{38}	CCCC ring puckering (τ(CC))	$S_{38} = \tau_3 - \tau_5 + \tau_4 - \tau_6$
A″	ν_{39}	CCCC ring puckering (τ(CC))	$S_{39} = 2\tau_1 - \tau_3 - \tau_5 + 2\tau_2 - \tau_4 - \tau_6$

[a] Symmetry coordinates are not normalized.

1634 cm^{-1} as obtained from RHF, MP2 and B3LYP levels at 6-31G(d) basis set, respectively. Accordingly, isomer **1** is considered a transition state and therefore eliminated.

The depolarization measurements were incomplete due to experimental obstacles [17], the very weak spectral features denoted by number 1 for Raman intensity were reported as depolarized bands. On the other hand, these dp bands are barely observed at 3178/3142 and 3142/3132 cm^{-1} (d_0/d_3) in the Raman liquid spectrum which render the reported dp ratios uncertain. The vibrational assignments of 2ATP (d_0 and d_3) are introduced in Table 1, where the calculated vibrational frequencies are in close proximity to experimental values. The overall percentage deviations of experimental vs calculated ones about 5%. To isolate the SH and NH_2 fundamentals, we have reproduced MP2 (Table 1) and B3LYP (Supplementary Table B) frequencies at 6-31G(d) basis set for $HSC_6H_4NH_2$ and $DSC_6H_4ND_2$ to observe the ND_2 and/or SD shifts for the *deuterated* 2ATP.

The calculated Raman intensities for υ_{3-6} are relatively high, therefore the recorded very weak (vw) bands at 3178, 3142 (d_0) and 3176, 3132 cm^{-1} (d_3) should be overtones. Similar to 2AP, the four CH stretching modes of 2ATP (d_0) are assigned to the observed very strong (vs) bands at 3068 (υ_3) and 3047 (υ_4) with a medium shoulder at 3010 cm^{-1} (υ_5 and υ_6). These three bands are little bit shifted in the deuterated isotopomer ($DOC_6H_4ND_2$) in agreement with Griffith [17], see Fig. 1 and Table 1.

The vibrational assignments of the NH_2/ND_2 stretching modes in 3AP (Table 1) were supported by the ratios of $\upsilon_{as}ND_2/\upsilon_{as}NH_2$ (0.73) and $\upsilon_sND_2/\upsilon_sNH_2$ (0.73) in agreement with ~0.74 and 0.72, respectively, [19]. Therefore, the observed medium Raman band (R_S) at 3353 cm^{-1} (υ_1 and υ_2) is assigned to υ_{as} and υ_s NH_2 modes shifted to 2494 (sh) and 2446 (m) for ND_2 stretches, respectively. The *gauche*-2 (**11**) and *trans* (**8**) conformations are expected to posses N···H and S···H inter- and intramolecular hydrogen bonding interactions in agreement with experimental observations [15], see Fig. 4 and Table 2.

The observed band at 1610 (m)/1610 (vs) [IR_s/R_s] scaled at 1648 cm^{-1} undergo significant shifting to 1130 (w)/1130 (vs) [IR/R] scaled at 1158 for the d_3 isomer. As a consequence the previous bands are assigned straightforward to NH_2 and ND_2 scissors mode (υ_8), respectively, which is consistent with ~1600 cm^{-1} reported for 2AP [17], 3AP [12], *o*-, *m*- and *p*-chloroanilines [52] and 2-amino-5-methylphenol [53].

Griffith has already assigned the CC ring stretches to the observed Raman bands at 1586, 1572, 1480, 1448, 1290 and 838 cm^{-1}. The observed bands at 1572 and 1480 cm^{-1} [17] are consistent with MP2 scaled/observed frequencies at 1613/1585 and 1606/1572 cm^{-1}. On the other hand, the reported bands at 1480 and 1448 are not consistent with the calculated intensities as well as the PEDs. Moreover, CH in-plane deformation (υ_{11}) should be more intense in IR spectrum (calc. IR intensity is 55.9 kcal/mol). Accordingly, the observed bands at 1481 (d_0) and 1476 (d_3) are assigned to δ_{ip}(CH) (υ_{11}) rather than CC stretch. The observed/scaled medium Raman bands at 1307/1329 and 1260/1287 cm^{-1} fit δ_{ip}(CH) (υ_{14}) and υ(CN) (υ_{15}) as well as the calculated Raman activities of 6.5 and 7.0 $Å^4$/amu, respectively, which contradicts the proposed CC stretch by Griffith and Koh [17]. The observed IR bands at 1304 (s) and 1287 (m,sh) match the calculated infrared intensities of 17.2 and 5.5 kcal/mol, respectively. However, the observed band at 1480 cm^{-1} with two shoulders at 1448 and 1400 cm^{-1} cover a range of ~100 cm^{-1}, where υ_{11}, υ_{12} (δ_{ip}(CH)) and υ_{13} (ring CC stretch) are expected. Hence, υ_{13} is assigned to the observed shoulder at 1400 cm^{-1} rather than an overtone devoted by Ref. [17] to weak band at 1390 cm^{-1} in IR_{liquid}. Additionally, the CC ring stretches were proposed earlier to the observed bands at 1290(m) and 1294(sh) cm^{-1} in the IR and R spectra of the liquid, respectively. Conversely, none of the CC stretches are expected in the region of 1350–1200 cm^{-1} (PEDs and the calculated frequencies in Table 1). The CC ring stretches υ_{19} and υ_{20} are assigned to the recorded bands at 1056 (w) and 1028 (vs) cm^{-1} for non-deuterated 2ATP d_0, respectively. In contrast, υ_{19} and υ_{20} are altered for the $-d_3$ isotopomer due to the mixing of S_{20} with $13S_{19}$ (C–C) and $11S_{28}$ (C–S). The 1028 (vs) cm^{-1} scaled at 1043 cm^{-1} with relatively high Raman activity of (22.4 $Å^4$/amu) was incorrectly assigned to δ_{ip}(CH) [17], although no CH bending modes are expected among 1150–900 cm^{-1}. The Raman medium band recorded at 1088 cm^{-1} ($-d_0$) undergo lower frequency shift to 830 cm^{-1} ($-d_3$) corresponds with NH_2 and ND_2 twisting modes (υ_{18}), respectively. It is questionable that unscaled MP2 wagging frequencies at 875 (υ_{22}) and 865 (υ_{23}) cm^{-1} are below experimentally noticed bands by ~100 cm^{-1}. Nevertheless, the B3LYP values of 947 (υ_{22}) and 928 (υ_{23}) cm^{-1} verify better matching with observed bands at 973 and 940 cm^{-1}, respectively, in good agreement with Ref. [17].

The δ_{ip}(SH) (υ_{21}) scaled at 902 and 683 cm^{-1} for $-d_0$ and $-d_3$ isotopomers, the later frequency could match the observed bands at 659 or 676 cm^{-1} in the IR spectrum of d_3. Moreover, neither IR nor Raman spectra of $-d_0$ 2ATP has corresponding features to the 659 cm^{-1}. Thus, δ_{ip}(SD) (υ_{21}) is assigned to the 659 compared to 911 cm^{-1} for the SH in-plane bending.

Table 6
B3LYP and MP2 unscaled force constants in mdyne/Å for 2-aminothiophenol (2ATP) and 2-aminophenol (2AP) at 6-31G(d) basis set

Internal coordinates[a]	Symbol	Scaling factor	(2ATP)[b] *Gauche-2* (**11**)		(2ATP) *Trans* (**8**)		(2AP) *Trans* (**8**)		(2ATP) *Gauche-1* (**7**)		(2AP)[c] *Gauche-1* (**7**)
			MP2	B3LYP	MP2	B3LYP	MP2	B3LYP	MP2	B3LYP	MP2
$\upsilon(C_1C_3)$	q_1	0.95	6.205	5.829	6.171	5.817	6.292	5.944	6.16	5.804	6.235
$\upsilon(C_3C_5)$	q_2	0.95	6.201	5.853	6.196	5.938	6.349	6.067	6.253	5.95	6.322
$\upsilon(C_5C_7)$	q_3	0.95	6.516	6.305	6.432	6.256	6.369	6.1	6.462	6.222	6.35
$\upsilon(C_7C_9)$	q_4	0.95	6.408	6.111	6.44	6.17	6.473	6.239	6.443	6.174	6.484
$\upsilon(C_9C_{11})$	q_5	0.95	6.465	6.188	6.466	6.162	6.339	6.046	6.412	6.143	6.319
$\upsilon(C_{11}C_1)$	q_6	0.95	6.315	6.04	6.35	6.047	6.46	6.241	6.294	6.051	6.478
$\upsilon(C_1S_2)$	T	1.00	3.675	3.29	3.676	3.286	6.358	6.187	3.701	3.319	6.402
$\upsilon(C_3N_4)$	R	1.00	6.598	6.602	6.488	6.386	6.683	6.496	6.5	6.376	7.046
$\upsilon(S_2H_{13})$	A	0.90	4.37	3.911	4.482	4.224	7.925	7.931	4.489	4.206	7.906
$\upsilon(C_5H_6)$	r_1	0.95	5.657	5.545	5.635	5.538	5.67	5.552	5.653	5.538	5.659
$\upsilon(C_7H_8)$	r_2	0.95	5.729	5.601	5.726	5.617	5.743	5.611	5.739	5.613	5.739
$\upsilon(C_9H_{10})$	r_3	0.95	5.761	5.637	5.744	5.631	5.757	5.63	5.751	5.628	5.756
$\upsilon(C_{11}H_{12})$	r_4	0.95	5.73	5.643	5.658	5.58	5.626	5.495	5.674	5.581	5.623
$\upsilon(N_4H_{15})$	a_1	0.90	7.138	6.896	6.162	7.062	7.322	7.238	7.145	7.066	7.555
$\upsilon(N_4H_{14})$	a_2	0.90	7.269	7.225	6.956	7.182	7.322	7.22	7.264	7.211	7.534
$\delta(N_4C_3C_1)$	ρ_1	1.0	1.565	1.576	1.506	1.5	1.499	1.481	1.496	1.48	1.471
$\delta(N_4C_3C_5)$	ρ_2	1.0	1.441	1.442	1.481	1.446	1.367	1.369	1.442	1.44	1.379
$\delta(S_2C_1C_{11})$	ε_1	1.0	1.342	1.334	1.418	1.368	1.458	1.455	1.367	1.354	1.453
$\delta(S_2C_1C_3)$	ε_2	1.0	1.455	1.428	1.464	1.396	1.513	1.505	1.429	1.391	1.491
$\delta(C_3C_5H_6)$	α_1	0.90	1.151	1.136	1.161	1.138	1.145	1.133	1.15	1.136	1.144
$\delta(C_7C_5H_6)$	α_2	0.90	1.155	1.144	1.158	1.14	1.148	1.137	1.153	1.14	1.148
$\delta(C_5C_7H_8)$	α_3	0.90	1.138	1.124	1.147	1.123	1.143	1.13	1.132	1.122	1.14
$\delta(C_9C_7H_8)$	α_4	0.90	1.138	1.124	1.149	1.124	1.145	1.133	1.135	1.124	1.144
$\delta(C_7C_9H_{10})$	α_5	0.90	1.129	1.118	1.136	1.118	1.13	1.118	1.131	1.119	1.128
$\delta(C_{11}C_9H_{10})$	α_6	0.90	1.128	1.115	1.129	1.115	1.126	1.114	1.129	1.116	1.124
$\delta(C_9C_{11}H_{12})$	α_7	0.90	1.146	1.135	1.166	1.143	1.143	1.133	1.152	1.141	1.142
$\delta(C_1C_{11}H_{12})$	α_8	0.90	1.159	1.151	1.165	1.141	1.125	1.115	1.151	1.14	1.124
$\delta(C_1S_2H_{13})$	λ	0.90	0.892	0.857	0.989	0.92	0.836	0.812	0.971	0.935	0.845
$\delta(C_3N_4H_{15})$	β_1	1.00	0.729	0.751	1.369	0.646	0.743	0.692	0.675	0.62	0.536
$\delta(C_3N_4H_{14})$	β_2	1.00	0.726	0.726	1.086	0.684	0.688	0.646	0.717	0.665	0.511
$\delta(H_{14}N_4H_{15})$	θ	0.95	0.632	0.582	1.4	0.593	0.605	0.558	0.628	0.575	0.444
$\gamma(C_3C_5H_6C_7)$	γ_1	1.0	0.38	0.426	0.386	0.428	0.378	0.431	0.385	0.431	0.373
$\gamma(C_5C_7H_8C_9)$	γ_2	1.0	0.419	0.471	0.421	0.452	0.401	0.444	0.404	0.45	0.399
$\gamma(C_7C_9H_{10}C_{11})$	γ_3	1.0	0.399	0.429	0.389	0.43	0.384	0.421	0.402	0.435	0.383
$\gamma(C_1C_{11}H_{12}C_9)$	γ_4	1.0	0.423	0.476	0.395	0.444	0.348	0.404	0.396	0.444	0.349
$\gamma(C_3C_1S_2C_{11})$	γ_5	1.0	0.515	0.556	0.586	0.504	0.592	0.648	0.461	0.408	0.587
$\gamma(C_1C_3N_4H_{15})$	γ_6	1.0	0.742	0.963	1.547	0.688	0.621	0.699	0.592	0.516	0.591
$\tau(C_{11}C_1C_3C_5)$	η_1	1.0	0.166	0.174	0.178	0.146	0.156	0.165	0.149	0.155	0.154
$\tau(C_1C_3C_5C_7)$	η_2	1.0	0.16	0.168	0.195	0.159	0.162	0.171	0.159	0.165	0.16
$\tau(C_3C_5C_7C_9)$	η_3	1.0	0.175	0.184	0.182	0.184	0.18	0.19	0.175	0.184	0.18
$\tau(C_5C_7C_9C_{11})$	η_4	1.0	0.18	0.187	0.183	0.187	0.186	0.193	0.18	0.187	0.186
$\tau(C_7C_9C_{11}C_1)$	η_5	1.0	0.178	0.187	0.179	0.183	0.179	0.188	0.175	0.183	0.179
$\tau(C_9C_{11}C_1C_3)$	η_6	1.0	0.179	0.19	0.161	0.166	0.166	0.178	0.16	0.169	0.166
$\tau(C_3C_1S_2H_{13})$	ζ_1	1.0	0.019	0.075	0.008	0.004	0.01	0.011	0.008	0.009	0.012
$\tau(H_{14}N_4C_3C_1)$	ζ_2	1.0	0.033	0.07	0.289	0.022	0.024	0.027	0.02	0.022	0.025

[a] Notations for internal coordinates: υ, stretch; δ, bending; γ, wagging and τ, torsion.
[b] *Gauche*-2 is unique for 2ATP only.
[c] B3LYP frequency calculations predicts an imaginary wavenumber for 2AP *gauche-1* (**7**), there for FC's are not listed above.

The $\delta_{as}(NH_2)$ mode is properly interpreted to the observed band at 1082 cm^{-1} [17]. Nevertheless, the $\delta_{as}(NH_2)$ could be twisting, wagging (out-of-plane) and/or rocking (in-plane) depending on the proposed symmetry coordinates (Table 5). The most intense IR band (309.9 kcal/mol) is chosen for NH_2 wag (υ_{26}) observed at 750 cm^{-1} (vs) which probably shifted as shoulder at 660 cm^{-1} for ND_2 wag. The υ_{24} (δ(CCC)) and υ_{25} (δ_{wag}(CH)) are well predicted at 857/859 and 849/806 per cm (B3LYP/MP2), which are consistent to the medium bands at 850 and 832 cm^{-1}, respectively. Other fundamentals υ_{27} (δ_{wag}(CH)) and υ_{29} (δ(CCC)) are in harmony with recorded one at 705 and 676 cm^{-1}, respectively, [17]. The observed medium band at 439 cm^{-1} in the IR liquid is absent in earlier study [17], this band could be assigned to CCC ring deformation (υ_{32}) which is 25 cm^{-1} apart from ring torsion (υ_{33}). The strong band at 475 (υ_{31}) better fits the CCN bending mode rather than υ(C–S) suggested by Ref. [17], which is supported by unscaled/scaled (478/475) frequencies for δ(CCN) (υ_{31}). Therefore, υ(C–S) is assigned to the observed bands at 676/680 (IR/R) cm^{-1}. The observed weak band at 433 cm^{-1} for 2ATP (d_3) coincides with and matches three fundamentals modes calculated at 443 (υ_{30}), 453 (υ_{31}) and 412 cm^{-1} (υ_{33}) which are separated by 30 cm^{-1}. The δ(CCC) (υ_{35}) predicted at 376/344 (unscaled/scaled) is recorded at 366 (vw) cm^{-1} in Roman solid.

The SH and SD torsion modes (υ_{34}) are observed at 373 (scaled at 374 cm^{-1}) and 252 (calculated at 263 cm^{-1}) in agreement with Ref. [17]. While, the observed medium band at 262 cm^{-1} is preferred for ring puckering modes υ_{36} (estimated at 266 cm^{-1}) and υ_{37} (estimated at 239 cm^{-1}). The observed strong band at 172 cm^{-1} is assigned to δ_{wag}(CS) (υ_{39}) in addition to ring torsion (υ_{38}) expected at 166 and 143 cm^{-1}, respectively.

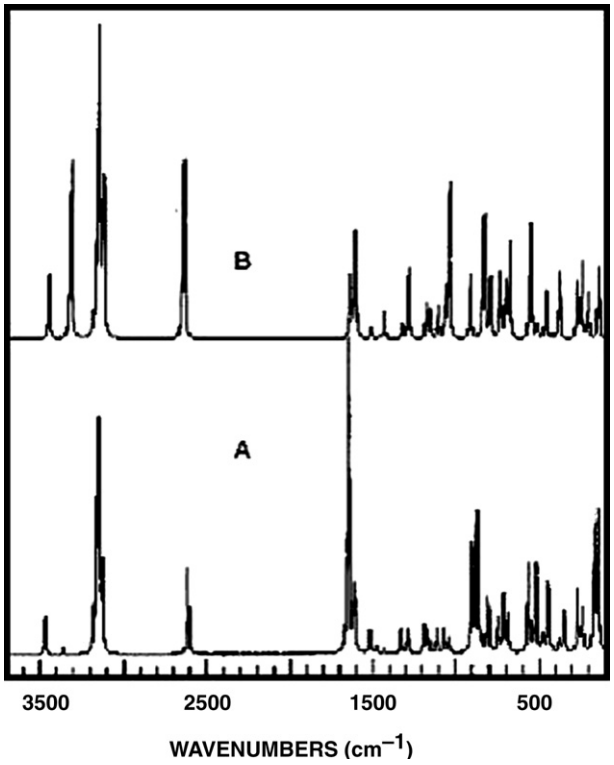

Fig. 9. Simulated Raman spectrum for 2-aminothiophenol utilizing MP2/6-31G(d) scaled frequencies; (A) *gauche-2* (**11**); (B) *trans* (**8**).

Acknowledgements

T.A.M. sincerely thanks Professor James R. Durig, Chemistry Department, College of Arts and Sciences, University of Missouri, Kansas City, MO 64110, USA, for giving him the opportunity to use G- and F-matrix programs to calculate FCs in internal coordinates and PEDs. The authors also wish to thank the National Institute of Standards and Technology (NIST), http://srdata.nist.gov.

Appendix A. Supplementary data

Supplementary data associated with this article can be found, in the online version, at doi:10.1016/j.theochem.2008.06.021.

References

[1] W. Plewska, M.R. Vigt, M.O. Magnussen, R.J. Behm, J. Phys. Chem. 103B (1999) 10440.
[2] Z. Quan, S. Chen, Y. Li, X. Cui, Corros. Sci. 44 (2002) 703.
[3] M.A. Ali, C.M. Haroon, M.N. Uddin, S.M.H. Majumder, M.T.H. Tarafder, M. Khair, Trans. Met. Chem. 17 (1992) 133.
[4] M.T.H. Tarafder, A.M. Ali, M.S. Elias, K.A. Crouse, S. Silong, Trans. Met. Chem. 25 (2000) 706.
[5] K. Sorasaenee, J.R. Galan-Mascaros, K.R. Dunbar, Inorg. Chem. 41 (2002) 433.
[6] T.A. Mohamed, J. Mol. Struct. (THEOCHEM) 179–192 (2005) 713.
[7] A. Alparone, A. Millefiori, S. Millefiori, J. Mol. Struct. (THEOCHEM) 640 (2003) 123.
[8] V.K. Yadav, A. Yadav, R.A. Poirier, J. Mol. Struct. (THEOCHEM) 186 (2005) 101.
[9] S. Kunimra, T. Ohsaka, N. Oyama, Macromolecules 21 (1988) 894.
[10] C. Barbero, J.J. Silber, L. Sereno, J. Electroanal. Chem. 291 (1990) 81.
[11] J.R.B. Gomes, M.A.V. Da Silva, Int. J. Quantum Chem. 101 (2005) 860.
[12] Y. Buyukmurat, S. Akyuz, J. Mol. Struct. 744–747 (2005) 921. themo 2AM.
[13] Y. Song, Spectrochim. Acta 67 (2007) 1164.
[14] J.C. Evans, Spectrochim. Acta 16 (1960) 428.
[15] P.J. Krueger, Tetrahedron 26 (1970) 4753.
[16] M.A. Palafox, M. Gill, J.L. Núñez, Vib. Spectrosc. 6 (1993) 95.
[17] W.P. Griffith, T.Y. Koh, Spectrochim. Acta 51A (1995) 253.
[18] C.Y. Panicker, H.T. Varghese, A. John, D. Philip, K. Istvan, G. Keresztury, Spectrochim. Acta 58A (2002) 281.
[19] U.A. Soliman, A.M. Hassan, T.A. Mohamed, Spectrochim. Acta 68A (2007) 688.
[20] M.J. Frisch, G.W. Trucks, H.B. Schlegel, G.E. Scuseria, M.A. Robb, J.R. Cheeseman, V.G. Zakrzewski, J.A. Montgomery Jr., R.E. Stratmann, J.C. Burant, S. Dapprich, J.M. Millam, A.D. Daniels, K.N. Kudin, M.C. Strain, O. Farkas, J. Tomasi, V. Barone, M. Cossi, R. Cammi, B. Mennucci, C. Pomelli, C. Adamo, S. Clifford, J. Ochterski, G.A. Petersson, P.Y. Ayala, Q. Cui, K. Morokuma, D.K. Malick, A.D. Rabuck, K. Raghavachari, J.B. Foresman, J. Cioslowski, J.V. Ortiz, A.G. Baboul, B.B. Stefanov, G. Liu, A. Liashenko, P. Piskorz, I. Komaromi, R. Gomperts, R.L. Martin, D.J. Fox, T. Keith, M.A. Al-Laham, C.Y. Peng, A. Nanayakkara, C. Gonzalez, M. Challacombe, P.M.W. Gill, B. Johnson, W. Chen, M.W. Wong, J.L. Andres, C. Gonzalez, M. Head-Gordon, E.S. Replogle, J.A. Pople, Gaussian 98, Revision A.7, Gaussian, Inc., Pittsburgh PA, 1998.
[21] W.J. Hehre, L. Radom, P.V.R. Schleyer, J.A. Pople, *Ab initio* Molecular Orbital Theory, Wiley, New York, 1986.
[22] C. Moller, M.S. Plesset, Phys. Rev. 46 (1934) 618.
[23] A.D. Becke, Phys. Rev. 38A (1988) 3098.
[24] C. Lee, W. Yang, R.G. Parr, Phys. Rev. 37B (1988) 785.
[25] A.D. Becke, J. Chem. Phys. 98 (1993) 5648.
[26] D.J. Fox, J.A. Pople, K. Raghavachari, L.A. Curtis, M. Head-Jordon, J. Chem. Phys. 90 (1989) 5622.
[27] P. Pulay, Mol. Phys. 17 (1969) 197.
[28] N.W. Larsen, F.M. Nicolaisen, J. Mol. Struct. 22 (1979) 29.
[29] S. Ashfaquzzaman, A.K. Pant, Acta Cryst. 35B (1979) 1394.
[30] J.R. Durig, Y.S. Li, J. Chem. Phys. 63 (1975) 4110.
[31] H.M. Badawi, J. Mol. Struct. (THEOCHEM) 726 (2005) 253.
[32] S. Portmann, H.P. Lüthi, Chimia 54 (2000) 766.
[33] F.A. Cotton, Chemical Applications of Group Theory, second ed., John Wiley & Sons, 1971.
[34] E.B. Wilson, J.C. Decius, P.C. Cross, Molecular Vibrations, McGraw Hill, New York, 1955 (republished by Dover, New York, 1980).
[35] H.J. Schachtshneider, Vibrational Analysis of Polyatomic Molecules, Parts V and VI, Technical Reports Nos. 231and 57, Shell Development Co., Houston, TX, 1964, 1965.
[36] Y. Yamauchi, M. Frisch, J. Gaw, H.F. Schaefer III, J. Chem. Phys. 84 (1986) 2262.
[37] A.P. Scott, L. Radom, J. Phys. Chem. 100 (1996) 16502.
[38] G.M. Kuramshina, F. Weinhold, J. Mol. Struct. 410–411 (1997) 457.
[39] H.P. Schlegel, J. Volkovski, M.D. Halls, Theor. Chem. Acc. 105 (2001) 413.
[40] A. Bondi, J. Phys. Chem. 68 (1964) 441.
[41] J.E. Huheey, E.A. Keiter, R.L. Keiter, Inorganic Chemistry: Principal of Structure and Reactivity, Collins, NY, USA, 1993.
[42] A. Almenningen, J. Brunvoll, M.V. Popik, L.V. Vilkov, S. Samdal, J. Mol. Struct. 118 (1984) 37.
[43] R. Kapreuta, Dissertation, Max–Plank Institute für Bioanorganische Chemi Mülheimander Ruhr, Germany, 2005.
[44] P. Pulay, X. Zhou, G. Fogarasi, in: R. Fausto (Ed.), Recent Experimental and Computational Advances in Molecular Spectroscopy, Kluwer Academic Publishers, The Netherlands, 1993, p. 99.
[45] M.A. Palafox, V.K. Rastogi, Spectrochim. Acta 58A (2000) 411.
[46] J.R. Durig, G.A. Guirgis, C. Zheng, T.A. Mohamed, Spectrochim. Acta 29A (2003) 2099.
[47] G.W. Chantry, in: A. Anderson (Ed.), Raman Effect, vol. 1, Marcel Dekker Inc., New York, 1971 (Chapter 2).
[48] M.J. Frisch, Y. Yamaguchi, J.F. Gaw, H.F. Schaefer, J.S. Binkley, J. Chem. Phys. 84 (1986) 531.
[49] R.D. Amos, Chem. Phys. Lett. 124 (1986) 376.
[50] P.L. Polavarapu, J. Phys. Chem. 94 (1990) 8106.
[51] T.A. Mohamed, G.A. Guirgis, Y.E. Nashed, J.R. Durig, Vib. Spectrosc. 30 (2002) 111.
[52] N. Sundaraganesan, B. Anand, B.D. Joshua, Spectrochim. Acta 67A (2007) 550.
[53] V.B. Singh, R.N. Singh, I.S. Singh, Spectrochim. Acta 22 (1966) 927.